Accepted Manuscript

Barrier layer characteristics of the Indian Ocean sector of the Southern Ocean during austral summer and autumn

Pranab Deb, Mihir K. Dash, Prem Chand Pandey

PII: S1873-9652(17)30142-1

DOI: 10.1016/j.polar.2018.04.007

Reference: POLAR 385

To appear in: *Polar Science*

Received Date: 28 December 2017

Accepted Date: 19 April 2018

Please cite this article as: Deb, P., Dash, M.K., Pandey, P.C., Barrier layer characteristics of the Indian Ocean sector of the Southern Ocean during austral summer and autumn, *Polar Science* (2018), doi: 10.1016/j.polar.2018.04.007.

Barrier layer characteristics of the Indian Ocean sector of the Southern Ocean during austral summer and autumn

Pranab Deb[a], Mihir K. Dash[b,*] and Prem Chand Pandey[b]

[a]School of Environmental Sciences, University of East Anglia, UK

[b]Centre for Oceans, Rivers, Atmosphere and Land Sciences, Indian Institute of Technology Kharagpur, India

* Corresponding author. Email address: mihir@coral.iitkgp.ernet.in

Abstract

Barrier layer in the Enderby Basin (EB) and the Australian Antarctic Basin (AAB) during late summer (December & January) and early autumn (February & March) are studied using temperature-salinity profiles collected between 1975 and 2012. A distinct difference in mixed layer depth is observed over the eastern (i.e. the EB) compared to western (i.e. the AAB) side of the Kerguelen Plateau (KP), with shallower mixed layer depths on the eastern side. Mixed layers show an increase from less than 50m to ~150m from south to north in the EB. During autumn, the wind strengthens and the upwelling over the eastern side of the KP (i.e. in the AAB) weakens, resulting in deeper mixed layers (~80m – 100m) compared to summer. During summer, deep barrier layer (BL) values (~50m or more) with porosity less than 0.3 was seen over the Chun Spur region. The fresher melt water from the EB brought by the Fawn trough current (FTC) across the KP may be responsible for the occurrence of BL over the region. During autumn, BL is spread over a much larger area around the Chun Spur, which could be attributed to the increase in the strength of FTC due to the intensification of wind over the region. A thorough study of BL condition over this region is required to understand the processes behind the discrepancies in sea ice conditions.

Key Words: Barrier layer, Kerguelen Plateau, Enderby Basin, Australian Antarctic Basin

1. Introduction

The growth and decay of sea ice not only play an important role in governing the upper ocean conditions over the marginal ice zone but affects the regional weather and global climate through energy balance too (Ackley et al., 2015; Moore et al., 2002; Rind et al., 1995). A great seasonal variability is present in Antarctic sea ice cover and a huge amount of fresh water is released into the ocean during melting of sea ice. This fresh melt water affects the upper ocean behavior in a regional as well as in basin scale (Shi and Lohmann; 2017). The density of polar water is found to be influenced mainly by salinity because small changes are observed in temperature (de Boyer Montégut et al., 2007). Influx of fresher melt water may result in shallow density mixed layer and formation of barrier layer. The impacts of salinity on the stratification of mixed layer in mid- and high latitudes have also been shown in studies by Reverdin et al., (1994) and Reverdin et al., (1997). Usually, the depth of halocline and thermocline are not always the same in the ocean. Instances where haloclines are shallower than the thermoclines (Lindstrom et al., 1987) give rise to an intermediate layer, called the "barrier layer" (Godfrey and Lindstorm, 1989). The air-sea heat and momentum exchanges are amply modified by the presence of barrier layer (Vialard and Delecluse, 1998). The barrier layer (BL) is an important parameter that influences the sea surface by trapping heat within the shallow mixed layer, resulting in positive SST anomalies (Vialard and Delecluse, 1998; Lewis et al., 1990). Furthermore, the modified heat content in the mixed layer in polar region might has an impact on the sea ice formation and vice versa. Thick BLs and strong vertical inversion have been detected over the Austral Ocean (south of Polar Front). However, due to deeper mixed layers in polar and subpolar regions, especially during winter, the climatic impacts of BL are questionable (Mignot et al., 2009). But, around the Antarctic divergence and south of Polar Front, the mixed layers are comparatively shallower during summer (Dong et al., 2008). So, the presence of BL could have a much profound effect on the air-sea interaction during summer.

The Indian Ocean sector of the Southern Ocean is unique among all the three major oceans, apparently not propagating the Antarctic circumpolar wave (Yuan and Martinson, 2000). The Kerguelen Plateau (KP), extended almost meridionally, acts as a barrier to the Antarctic Circumpolar Current (ACC) in this sector. The larger ACC transport is found to be deflected towards north, with a secondary transport through the Antarctic zone between Kerguelen Islands and Antarctica (Park et al. 1993). This gives rise to interesting regional circulation pattern over the region. The Deep Western Boundary Current flowing towards northwest direction along the eastern slope of the KP (Donohue et al., 1999; McCartney and Donohue, 2007) has been found to carry deep water from the Antarctic coast or from Princess Elizabeth Trough to as far north as 50.5°S (van Wijk et al., 2010). Van Wijk et al. (2010) found two distinct branches of Polar front to the immediate west of KP. Their study also found that the southern branch of Polar Front contributes to the Fawn Trough Current (FTC, identified by McCartney and Donohue, 2007). They also suggests that a possible southward shift of the southern branch of FTC to the east of KP is responsible for the advection of warmer water from north. The estimated transport over the eastern side of KP reflected a variability in the path and strength of both polar front and deep western boundary current. So, it is likely that interaction between these regional circulations and bathymetry of the region strongly influences the upper ocean behavior over the region. The upper ocean is generally represented by the halocline and thermocline.

This study is to investigate the presence of BL over the Indian Ocean sector of the Southern Ocean and the possible mechanisms of its formation in the context of regional circulation. The study tries to create a robust picture of the mixed layer and barrier layer distribution over the region. The study also calculates the 'permeability' or 'porosity' of the BLs (Mignot et al., 2009) to indicate how effective the barrier layers are. A thorough study can give us an insight into the impact of regional circulation on the upper ocean characteristics in this region.

2. Study area and data used

The study is conducted with temperature-salinity profiles collected between 1975 and 2012. The profiles are taken from World Ocean Dataset (WOD) 2009 at the National Oceanographic Data Center (NODC) (Boyer et al., 2009), the World Ocean Circulation Experiment (WOCE) (WOCE Data Product Committee, 2002) and the Argo database (Coriolis Global data Assembly Center, www.coriolis.eu.org). The profiles with spurious data are removed. The temporal distribution of different profiles is shown in Fig. 1.The sparsity of in situ data is evident before 1986; however, the number of observations increases gradually and with the introduction of Argo floats, the number of in situ observations shows a steady rise after 2003 (Fig. 1). The profiles are then subjected to standard tests, e.g., spike test, gradient test and density instability tests. These tests removed around 4% Conductivity-Temperature-Depth profiles (CTD), 6.88% Profiling Floats profiles (PFL), 0.34% Autonomous Pinniped Bathythermograph profiles (APB) and 2.27% Ocean Station Data profiles (OSD). At the end, 3948 profiles are taken for analysis.

The study area covers the Enderby Basin, the Australian Antarctic Basin, connected by Fawn trough region present in the Indian Ocean sector of the Southern Ocean. Major current and frontal systems and schematically presented in Fig. 2.

3. Profile characteristics

The profiles to the south of the Polar Front (PF) over the study region are associated with the presence of Winter Water (WW) between 100m and 300m depth ranges (Fig. 3(a)). The WW is the layer of cold winter temperature and is capped by warmer surface layer above it. Beneath this layer of WW, the presence of Upper Circumpolar Deep Water (UCDW) is seen, which has a temperature of around 2°C. The surface layer was found to be warmer than the UCDW layer. Salinity is more or less uniform over the surface layer, but increases gradually with depth. This temperature/salinity structure is a common occurrence to the south of PF (Fig. 3).

However, some of the profiles around the PF and to the north of it show the typical stratification with decreasing temperature and increasing salinity with depth. Fig. 3(a) shows the average temperature-salinity profile over the Enderby Basin (EB), while Fig. 3(b) shows the average profile over the Australian-Antarctic Basin (AAB). Comparatively more saline surface water (~34 psu) is observed over the AAB than the EB (~33.7 psu). The effect of saline and cold WW is less prominent in the AAB profiles (Fig. 3(b)).

3.1 Calculation of mixed layer and barrier layer depths

Previous studies (Brainerd and Gregg, 1995; Thomson and Fine, 2003) have indicated that temperature mixed layer/isothermal layer depth (ILD) and density mixed layer depth (MLD) calculated from a difference criteria gives more realistic measures. We follow the difference criteria used by Dong et al. (2008) since it gives a stable measurement of mixed layers over the Southern Ocean. The temperature criteria is taken as $\Delta T = 0.2°C$; i.e. the ILD is defined as the depth at which the temperature falls below the surface temperature (Ts) by 0.2°C. The MLD is defined as the depth at which the density is increased by 0.03 kg m-3 (i.e. $\Delta\rho = 0.03$ kg m-3) from that of the surface value (ρs). Average temperature (Ts) /density (ρs) of top 10m layer is taken as reference. Using these criteria ILD, MLD and barrier layer thickness (BL = ILD - MLD) are calculated from the individual temperature and salinity profiles. These values from individual profiles are then used to generate the bi-monthly conditions of ILD, MLD and BL at 1° × 1° resolution over the study area for the austral summer (i.e. December-January months) and austral autumn (i.e. February-March months) periods. de Boyer Montégut et al. (2007) determined BL depth as the median of all available observations in each grid. However, Mignot et al. (2009) argued that BLs show intermittent nature in both space and time and the BL distribution within a grid cell is skewed towards high values rather than being Gaussian in nature. So taking median of all the observation (as in de Boyer Montégut et al., 2007) underestimates the BL thickness. In this study BL is estimated by taking the thickness median of the stations with effective BL values only, satisfying the following criteria (Mignot et al. 2009):

BL>5m

BL>10% (ILD)

To make the study more statistically robust, we calculated median at the grid points having at least 5 stations.

The appearance and disappearance of BLs are associated with their own time and space scale of formation. BL can effectively modify the air-sea interaction if it is sufficiently continuous in space and time. To find the effective BL present over time, Mignot et al. (2009) introduced the term 'barrier layer porosity' to specify the permeability of BLs. First the 'persistence' of BLs (R) is calculated. It is defined as the ratio of the number of stations showing BL to the total number of stations. Then barrier layer porosity is calculated as '1-R'. It gives an idea about how effective the BL is. The MLD, ILD and BL climatologies for austral summer and austral autumn had variabilities resulting from noisy nature of observations. So, we applied smoothing, similar to that used by de Boyer Montégut et al. (2004). The regions with no data points were filled with Laplace Interpolation, which is a specialized interpolation technique for restoring missing data on a two or three dimensional grid. The technique does not change any known values. It is fast and uses linear extrapolation. Averaged Ekman pumping and Ekman transport for summer (December-January) and autumn (February-March) periods are calculated using QuikSCAT monthly wind stress data (Pegion et al., 2000) over the study region.

4. Results and discussions

The Indian Ocean sector of the Southern Ocean is broadly divided into two regions (i) Enderby Basin (EB) and (ii) Ausralian Antarctic Basin (AAB). Kerguelen Plateau (KP) separates these two basins. Both the basins are different in their water mass characteristics and sea ice extent/area. Generally sea ice edge is present more towards equator in the EB than that in the AAB.

The ILD for austral summer is shown in Fig. 4(a). The depth of ILD is more in the EB than that in the AAB covered within the study domain. Maximum ILD is found to be of the order of 130m in the EB. Over the western part of the KP, the region south of 56°S is associated with ILD values less than 60m over the longitude range 50°E-70°E (Fig. 4(a)).

A distinct difference in ILD and MLD over the eastern and western part of the KP is observed. The average ILD value over the eastern part is found to be of the order of 70m (Fig. 4(a)). The distribution of MLD over the study region is shown in figure 5(a). The MLD values follow similar distribution over the region as that of ILD, with deeper values to the north and shallower values to the south. Deeper ILD (~120m) and MLD values (>150m) are found on the western side of Heard Island in the KP (Fig. 4(a) & 5(a)). It may be the result of bathymetry driven downwelling. MLD values are found to be shallower (<50m) compared to ILD values over the Chun Spur region (to the east of Heard Island) and may be caused by the advection of melt water. ILD and MLD over the Weddell gyre region (20-40°E) show moderate values with values less than 70m to the south of 56°S and reaching up to 120m to the north of it.

During summer almost the whole study area shows negative wind stress curl (Fig. 6(a) for wind stress curl) signifying that upwelling persists over the region. It is supported by positive Ekman pumping (Fig. 7(a)).

Shallower thermocline present in the EB between 60-52°S latitude belt may be attributed to strong upwelling (Ekman pumping >1.5x10-7) (Fig. 7(a)) and is responsible for shallower MLD and ILD values (Fig. 4(a) & 5(a)). Deeper values of MLD are seen closer to the northern boundary of the study area with some of the values exceeding 150m (Fig. 5(a)), which may be attributed to the stronger wind (Fig. 6(a)) and downwelling observed over the region (Fig. 7(a)). Thicker ILD and MLD are noticed on the western side of the KP than on the eastern side (Fig. 4(a) and 5 (a)). This may be due to the complex interaction between the current and topography of the region.

Before analyzing the barrier layer over a particular region, we first looked at the 'barrier layer porosity' distribution over the study area (Fig. 8(a)). The BL porosity of 0.3 or less is found to be spread over a ~2˚x2˚ region. Separate monthly studies are performed to understand the situation during each month of the December and January. The BL porosity is found to be less than 0.3 during both December and January months. During February, thick BL with porosity less than 0.3 is observed over 75-80°E belt, to the south of 57°S (no observations present over Chun Spur region during this month). During March, thick BLs with porosity less than 0.3 is observed over the Chun Spur and over the 60-80°E longitude belt, south of 58°S. However, the interpretation of BL porosity in determining its effect on air-sea interaction is important and it is sensitive to both temporal and spatial resolution of the grid. The Chun Spur region shows a porosity of 0.3 or less during both the bimonthly periods. Since a bimonthly data is presented, a porosity of ~0.3 means that BL can appear more than 70% of the time i.e., more than three fourth of the two month period.

Thus, the BL is spatially spread over a larger region and more than 70% of the profiles over the region show deep BL. However, it cannot be specified whether BL is present continuously over the entire two months period or over a comparatively smaller period (say, the last 15 days of the bimonthly cluster). This is because the temperature salinity profiles are not be available over the whole period. Hence, in this case, the porosity of 0.3 is present during both the months and spread over a larger (~2˚x2˚) region over Chun Spur. So, this value of BL porosity (i.e., 0.3) is taken to be sufficient to affect the air-sea interaction over the region. The concept of BL porosity is inseparable from both time and space scales and a shorter temporal resolution would be helpful in understanding the BL persistence better. But unavailability of continuous data makes this impossible over the study area. The region surrounding Chun Spur shows thick BL values (~50m or more) (Fig. 9(a)) with porosity less than 0.3 (Fig. 8(a)) during summer. This indicates a strong and effective BL. The presence of strong Fawn Trough current (FTC) to the south of Heard Island across the KP, which brings fresher melt water from EB to the Chun Spur region (Rouqet et al., 2009), is responsible for the occurrence of BL over the region.

Additionally, wind-induced downwelling (~ -1x10-6, Fig. 7(a)) is observed over the Chun Spur region, which is associated with deeper ILDs (~70 m) compared to the neighbouring area (Fig. 4(a)). But fresher EB water carried by the FTC may play a role in the formation of BL. Apart from this, a small region between 30°E-40°E, south of 57°S shows barrier layer with depth between 20m and 40m and porosity between 0.2-0.6. The region is associated with a circular patch of comparatively weaker WS curl values (~-1.5 x10-7, Fig. 6(a)) during summer, which may reduce the upwelling over this small region. The wind-driven northward advection of fresher melt water (Fig. 7(a)) creates a shallow density stratified layer, thus resulting in positive BL values there.

4.1 Barrier layer characteristics during austral autumn

Fig. 4(b) shows the ILD distribution during autumn. Deeper ILD values (120m-160m) are seen to the north of 57°S over the western side of the plateau. However, the eastern part of the study area shows ILD values between 80m and 100m. MLD distribution over the study region is shown in Fig. 5(b). Both ILD and MLD are found to be thicker during autumn than during summer. During autumn, the wind is intensified over the study region (Fig. 6(b)) compared to that during summer. This results in an increase in the wind-induced downwelling. Strong downwelling (of magnitude >1.5 x10-7 m/s) can be seen between 50°S-53°S (Fig. 7(b)). The western escarpment of the Heard Island exhibits bathymetry-driven downwelling and hence comparatively deeper ILD/MLD values (Fig. 4(b) & 4(b)). Over the Weddell Gyre region, the ILD and MLD values are deeper (>70m) to the north of 56°S while shallower (<50m) to the south of it; this is associated with a shift in wind stress curl and Ekman pumping values across 56°S (with strong upwelling to the south of 56°S) over the region (Fig. 6(b)). Shallower MLDs (<30m) appear over the Chun Spur region and the eastern side of the plateau over the southern belt (south of 58°S) (Fig. 5(b)). The stratification caused by the advection of melt water might be responsible for the shallow MLDs.

BL is spread over a much larger area around Chun Spur during autumn, which could be the result of increase in the strength of FTC due to the intensification of wind over the region. Porosity values reach as low as 0.2 during this season and are spread over a larger area compared to summer period (Fig. 8(b)). The BL layer in this case is much more persistent. Another region south of 58°S and over the eastern part of the study area shows thicker BL values (16m-50m) (Fig. 9(b)) with porosity ranging from 0.2 to 0.6 (Fig. 8(b)). Also, the eastern side of southern KP is associated with a bathymetry-driven northward protrusion of sea ice cover, which is why fresher melt water reach a much northward extent along the eastern slope of KP (figure not shown) and BL formation is seen there (Fig. 9(b)). Previous studies (Park et al., 1993) have shown that sea ice over the eastern side of the plateau melts completely only at the end of February, thus producing more melt water during February-March months. This late melting on the eastern side may be the reason why no significant BL was observed during December-January months. Apart from these two prominent regions, a region to the south of 57°S, 20°E-30°E (Weddell gyre region) exhibits BL with values ~50m and porosity 0.3-0.6 (Fig. 9(b) & 8(b)). The melt water carried by the eastern limb of the Weddell gyre might be responsible for the observed BL. Another region of BL formation is to the south of Elan Bank ~58°E-75°E, with BL values between 8m and 50m and porosity<0.2. The region shows a weaker upwelling (~1-1.5x10-6 m/s, Fig. 7(b)) and deeper ILDs (70m – 110m) compared to neighbouring areas (Fig. 4(b)). A strong wind-driven Ekman transport (Fig. 7(b)) causes northward advection of melt water and results in shallower MLDs (<70m, Fig. 5(b)), which is responsible for the BL formation over the region (Fig. 9(b)).

Above observations suggest that a persistent and thick BL appears consistently over the Chun Spur region during both the seasons and is likely to have a strong influence on the air-sea interaction over the region.

The major current system which flows across these two regions is the FTC. McCartney and Donohue (2007) suggested that the surface expression of the Polar Front (SPF, defined by Holliday and Read, 1998) to the west of FT results in a strong eastward flow through the trough. This was later confirmed by van Wijk et al. 2010 (hereafter, vW10), suggested that cold and fresh water from the south fill up the trough. Park et al. (2008) also suggested the FT as a pathway for the advection of southern cold water towards northern plateau. The FTC turns northward on the eastern end of the trough and then meanders to the east of the KP and moves south-east in the AAB (Roquet et al. 2009). This is responsible for the southward advection of warm sub-polar water in the AAB (vW10). A schematic diagram of the regional circulation over the Chun Spur region (following vW10) is shown in Fig. 2. The broad circulation (Fig. 2) suggests that, on exiting the FT, some streamlines move briefly to the northwest after passing Chun Spur and then turns offshore while some streamlines directly go offshore near Chun Spur after exiting the trough. Strong surface geostrophic flow indicates that cold and fresh surface water can spread over a greater zonal extent. vW10 hypothesized that the Northern Polar front (subsurface expression of the Polar Front) meets the SPF on the eastern side of the trough.

The confluence zone, however, shows wide variability in its location (Park et al. 2008, vW10), indicating that the path and strength of SPF/FTC shows great variability as well. The transport estimates over the eastern KP (Speer and Forbes, 1994; Donohue et al. 1999) also reflects this variability.

The mean Ekman pumping and wind stress curl show that the Chun Spur is a downwelling region (Fig. 6 and 7), and thus associated with thicker ILD (Fig. 4) compared to the neighbouring areas over AAB. The presence of non-porous deep BLs (Fig. 9) in this region is attributed to the FTC, which brings fresher water over the region creating strong density stratified layers. During autumn, the region along the steep slopes of southern Heard Island also shows the presence of BL with low porosity (Fig. 9(b)); this indicates the importance of topography steered FTC in carrying fresher southern water up to the northern plateau in and around the Chun Spur region. However, the strength and transport of FTC could be an important variable.

5. Summary

The ILDs, MLDs and BLs in the EB and the AAB during late summer and early autumn are studied using temperature-salinity profiles collected between 1975 and 2012. A distinct difference in mixed layer depth over the eastern (EB) and western (AAB) side of the KP is observed, with shallower mixed layer depths on the eastern side. A strong upwelling over 60°S-52°S latitude belt on the eastern side may be responsible for the shallower depth. Overall, the region to the north of 56°S is seen to be associated with deeper mixed layers due to the influence of the ACC and strong wind-induced downwelling. The region to the south shows strong upwelling under the influence of Antarctic divergence and hence the region is associated with shallower mixed layer. Over the EB, mixed layers show an increase from less than 50m to ~150m from south to north. During autumn, the wind strengthens and the upwelling over the eastern side of KP (i.e. in the AAB) weakens, resulting in deeper mixed layers (~80m – 100m) compared to summer. On the western side of KP (i.e. in the EB), at southern latitudes (to the south of 58°S) mixed layers are shallower than 50m, while to the north of it, wind-induced mixing results in deeper layers with depth ranging from 100m to 160m. During summer, deep BL values (~50m or more) with porosity less than 0.3 was seen over the Chun Spur region. The fresher melt water from the EB brought by the FTC across the KP may be responsible for the occurrence of BL over the region. During autumn, BL is spread over a much larger area around the Chun Spur, with porosity values as low as 0.2, which could be the result of increase in the strength of the FTC due to the intensification of wind over the region. A thorough observational and modeling study of BL condition over the IOS will further enhance the understanding of the processes behind the discrepancies in air-sea interaction and sea ice conditions over the region.

Acknowledgement:

The authors are grateful to the guest editors for their invitation. The authors are thankful to the Director, National Centre for Antarctic and Ocean Research, Goa, India for his encouragement during the course of this work.

References

Ackley, Stephen F., Xie, H., and Tichenor, Elizabeth A., 2015. Ocean heat flux under Antarctic sea ice in the Bellingshausen and Amundsen Seas: two case studies, Annals of Glaciology. 56 (69). doi: 10.3189/2015AoG69A890

Boyer, T. P. Antonov, J. I., Baranova, O. K., Garcia, H. E., Johnson, D. R., Locarnini, R. A., Mishonov, A. V., O‟Brien, T. D., Seidov, D., Smolyar, I. V., and Zweng, M. M., 2009. World Ocean Database 2009. S. Levitus, Ed., NOAA Atlas NESDIS 66, U.S. Gov. Printing Office, Wash., D.C., 216, DVDs.

Brainerd, K. E., and Gregg, M. C., 1995. Surface mixed and mixing layer depths. Deep Sea Res. Part I. 9, 1521 – 1543.

de Boyer Montégut, C., Mignot, J., Lazar, A., and Cravatte, S., 2007. Control of salinity on the mixed layer depth in the world ocean: 1. General description. J. Geophys. Res. 112, C06011, doi:10.1029/2006JC003953.

Dong, S., Sprintall, J., Gille, S. T., and Talley, L., 2008. Southern Ocean mixed layer depth from Argo float profiles. J. Geophys. Res. 113, C06013, doi:10.1029/2006JC004051.

Donohue, K. A., Hufford, G. E., and McCartney, M. S., 1999. Sources and transport of the deep western boundary current east of the Kerguelen Plateau. Geophys. Res. Lett. 26, 7, 851–854.

Godfrey, J. S., and Lindstrom, E. J., 1989. The heat budget of the equatorial western Pacific surface mixed layer. J. Geophys. Res. 94, 8007– 8017.

Lewis, M. R., Carr, M. E., Feldman, G. C., Esaias, W., and McClain, C. 1990. Influence of penetrating solar radiation on the heat budget of the equatorial Pacific Ocean. Nature. 347, 543–545.

Lindstrom, E., Lukas, R., Fine, R., Firing, E., Godfrey, S., Meyers, G., and Tsuchiya. M., 1987. The Western Equatorial Pacific Ocean Circulation Study. Nature. 300, 533– 537.

McCartney, M. S., and Donohue, K. A., 2007. A deep cyclonic gyre in the Australian– Antarctic Basin. Progress in Oceanography. 75,4, 675–750.

Mignot, J., Lazar, A., and Lacarra, M., 2012. On the formation of barrier layers and associated vertical temperature inversions: A focus on the northwestern tropical Atlantic. J. Geophys. Res. 117, C02010, doi:10.1029/2011JC007435.

Mignot, J., Montégut, C. D. B., and Tomczak, M., 2009. On the permeability of barrier layers. Ocean Science Discussions. 6, 1, 799.

Moore, G.W.K., Alverson, K., Renfrew, I.A., 2002. A reconstruction of the air–sea interaction associated with the Weddell Polynya, J. of Physical Oceanography. 32(6), 1685– 1698, 10.1175/1520–0485(2002)032<1685:AROTAS>2.0.CO;2

Park, Y. H., Gamberoni, L., and Charriaud, E., 1993. Frontal structure, water masses, and circulation in the Crozet Basin. J. Geophys. Res. 98, C7, 12361–12385.

Park, Y. H., Roquet, F., Durand, I., and Fuda, J. L., 2008. Large–scale circulation over and around the Northern Kerguelen Plateau. Deep Sea Res. Part II: Topical Studies in Oceanography. 55, 5, 566–581.

Parkinson, C. L. and Cavalieri, D. J., 2012. Antarctic sea ice variability and trends, 1979–2010. The Cryosphere. 6, 871–880, doi:10.5194/tc–6–871–2012.

Pegion, P. J., Bourassa, M. A., Legler, D. M., and O‟Brien, J. J., 2000. Objectively derived daily "winds" from satellite scatterometer data. Monthly Weather Review. 128, 3150– 3168.

Reverdin, G., Cayan, D., and Kushnir, Y., 1997. Decadal variability of hydrography in the upper northern North Atlantic in 1948–1990. J. Geophys. Res. 102(C4), 8505–8531, doi:10.1029/96JC03943.

Reverdin, G., Frankignoul, C., Kestenare, E., and McPhaden, M. J., 1994. Seasonal variability in the surface currents of the equatorial Pacific. J. Geophys. Res. 99, 20323–20344.

Rind, D., Healy, R., Parkinson, C., and Martinson, D., 1995. The role of sea ice in 2× CO_2 climate model sensitivity. Part I: the total influence of sea ice thickness and extent. J. Clim. 8(3), 449–463.

Roquet, F., Park, Y. H., Guinet, C., Bailleul, F., and Charrassin, J. B., 2009. Observations of the Fawn Trough Current over the Kerguelen Plateau from instrumented elephant seals. J. Marine Systems. 78(3), 377–393.

Shi, X., and Lohmann G., 2017. Sensitivity of open-water ice growth and ice concentration evolution in a coupled atmosphere-ocean-sea ice model. Dynamics of Atmospheres and Oceans. 79 , 10–30, https://doi.org/10.1016/j.dynatmoce.2017.05.003

Speer, K. G., and Forbes, A., 1994. A deep western boundary current in the South Indian Basin, Deep Sea Res. Part I: Oceanogr. Res. Pap. 41(9), 1289–1303.

Thomson, R. E., and Fine, I. V., 2003. Estimating mixed layer depth from oceanic profile data. Journal of Atmospheric and Oceanic Technology. 20, No. 2, 319–329.

van Wijk, E. M., Rintoul, S. R., Ronai, B. M., and Williams, G. D., 2010. Regional circulation around Heard and McDonald Islands and through the Fawn Trough, central Kerguelen Plateau. Deep Sea Res. Part I: Oceanographic Research Papers. 57, No. 5, 653–669.

Vialard, J., and Delecluse. P., 1998. An OGCM study for the TOGA decade. part 1: role of salinity in the physics of the western Pacific freshpool. J. Phys. Oceanogr. 28, No. 6, 1071–1088, doi: 10.1175/1520–0485(1998)028<1071:AOSFTT>2.0.CO;2.

Yuan, X., and Martinson, D.G., 2000. Antarctic sea ice extent variability and its global connectivity. J. Clim. 13, 1697–1717.

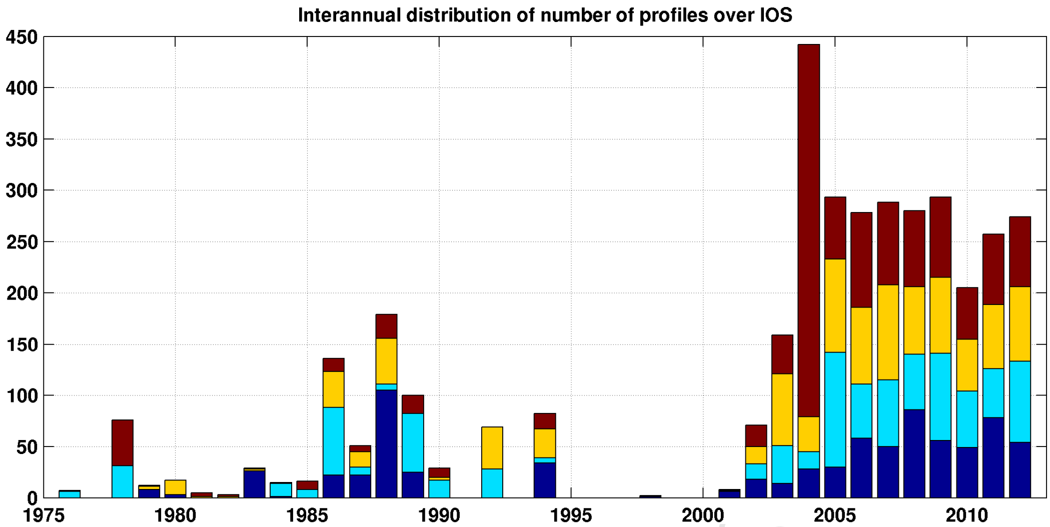

Fig. 1. Inter-annual variation of profile numbers with monthly distribution; blue part of the bar shows number of profiles in December, sky-blue part shows the same in January, yellow part shows the number of profiles in February while the red part represents the number of profiles in March for that particular year.

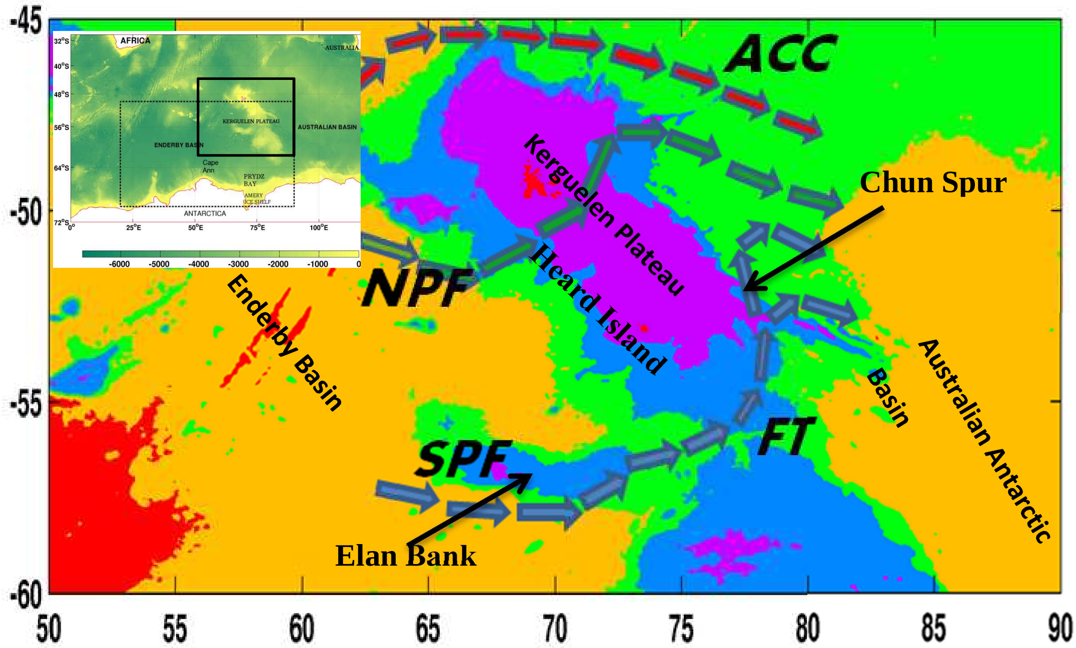

Fig. 2. The inner figure shows the study area is shown with a thick solid rectangular box. The colour bar represents the bathymetry of the region. The dashed box shows the Indian Ocean sector of the Southern Ocean Parkinson and Cavalieri (2012). The outer figure shows the schematic diagram of the circulation over the Fawn trough (FT) region (following van Wijk et al., 2010); red arrows show the Antarctic Circumpolar Current (ACC), green arrows show the Northern Polar Front (NPF) and blue arrows show the Southern polar Front (SPF).

(a)

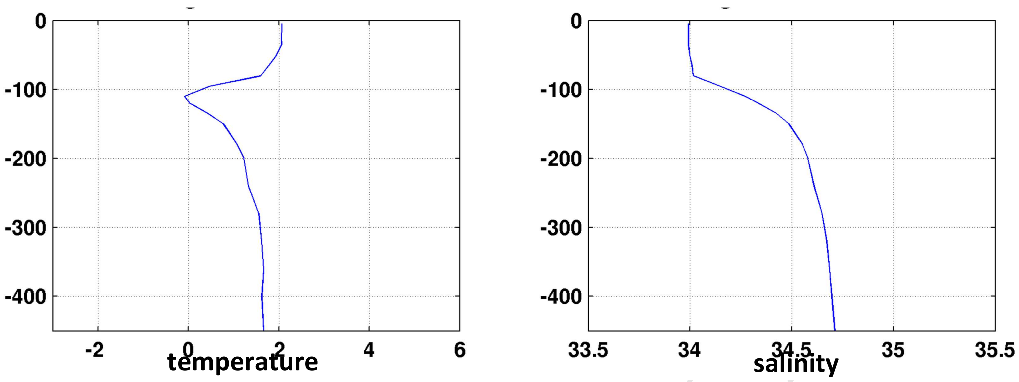

(b)

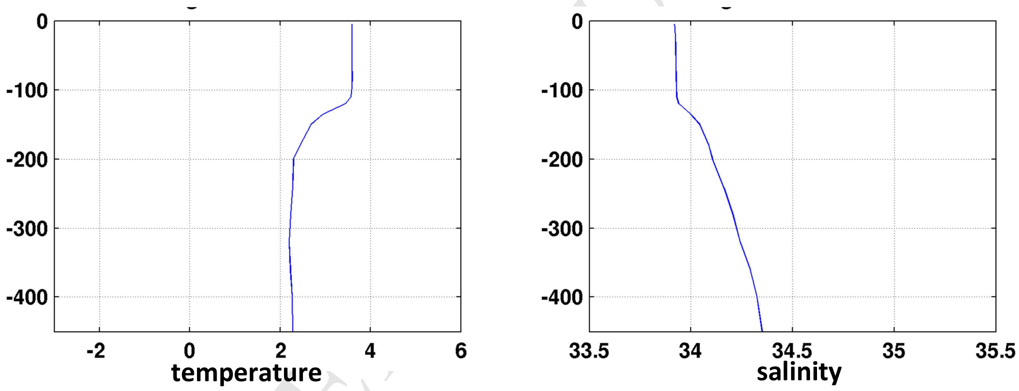

Fig. 3. Typical temperature (left) and salinity (right) profile over (a) the Enderby Basin and (b) over the Australian-Antarctic Basin for regions to the south of Polar front. Upper (lower) panel represent the EB (AAB).

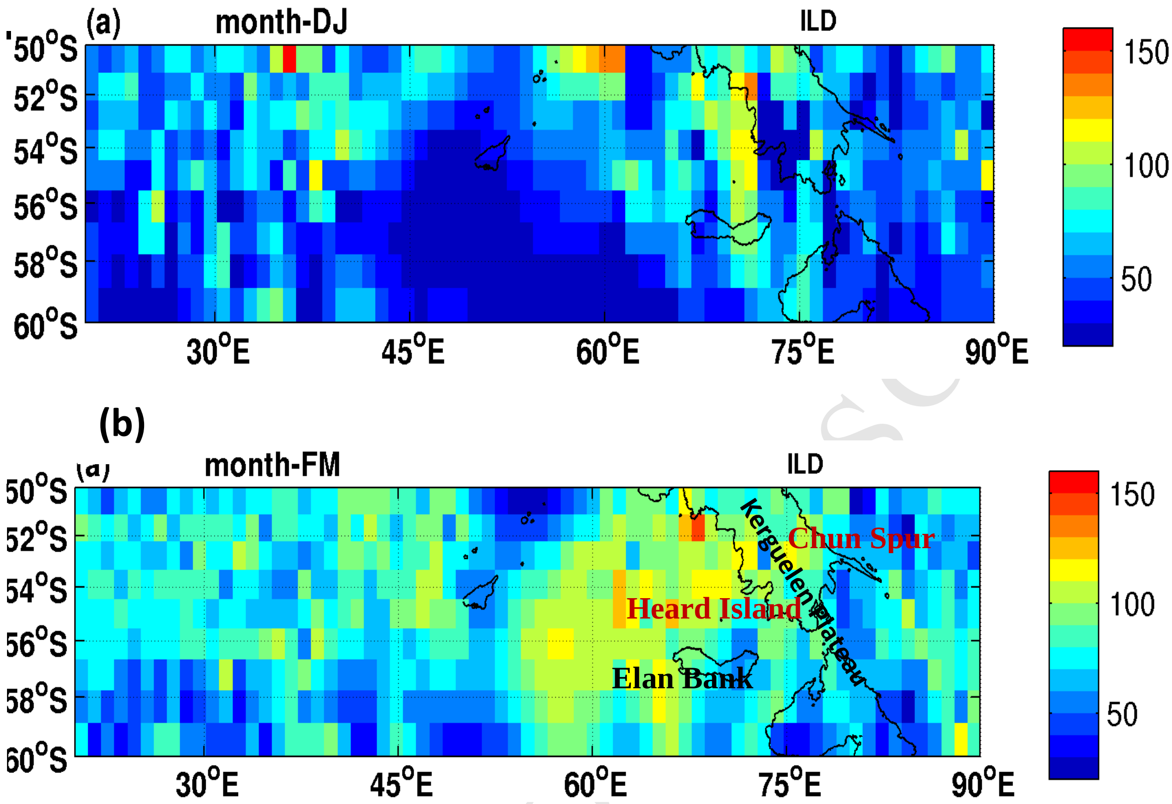

Fig. 4. Horizontal distribution of average isothermal layer depth (ILD, in m) calculated from in-situ observations between 1975 and 2012 for (a) summer (December-January) and (b) autumn (February-March) seasons over the study area.

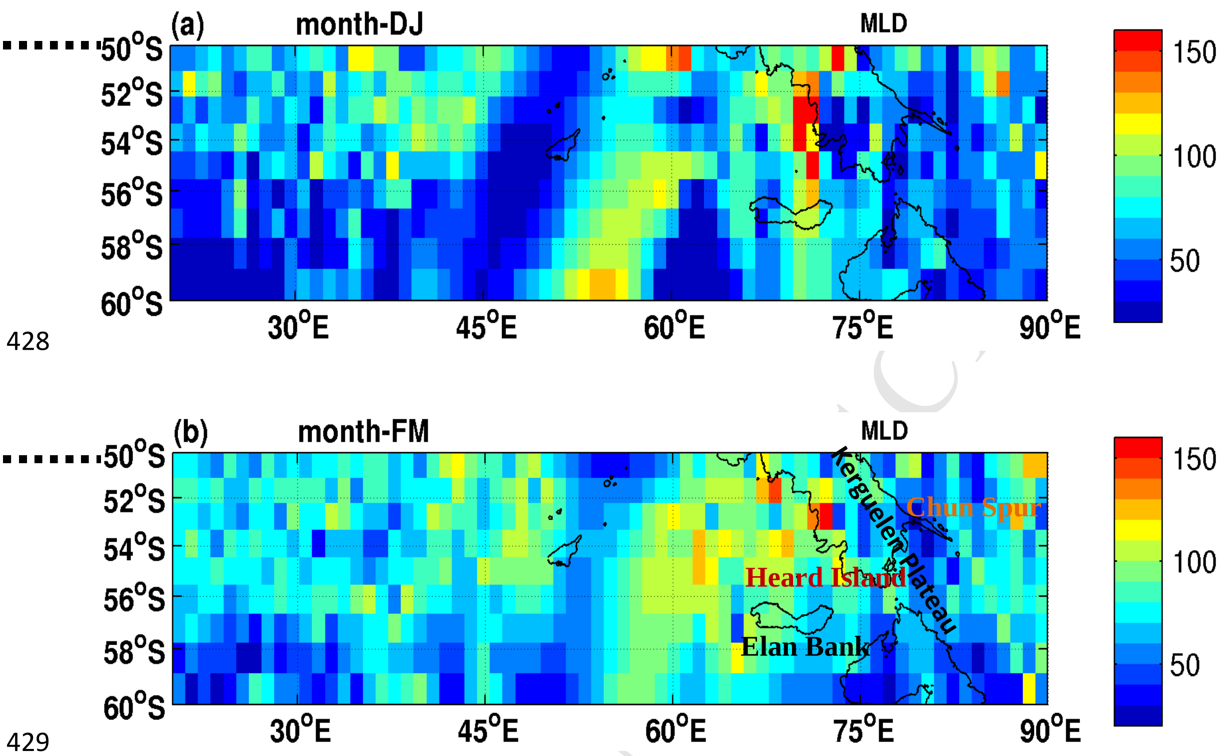

Fig. 5. Horizontal distribution of average density mixed layer depth (MLD, in m) calculated from in-situ observations between 1975 and 2012 for (a) summer (December-January) and (b) autumn (February-March) over the study area.

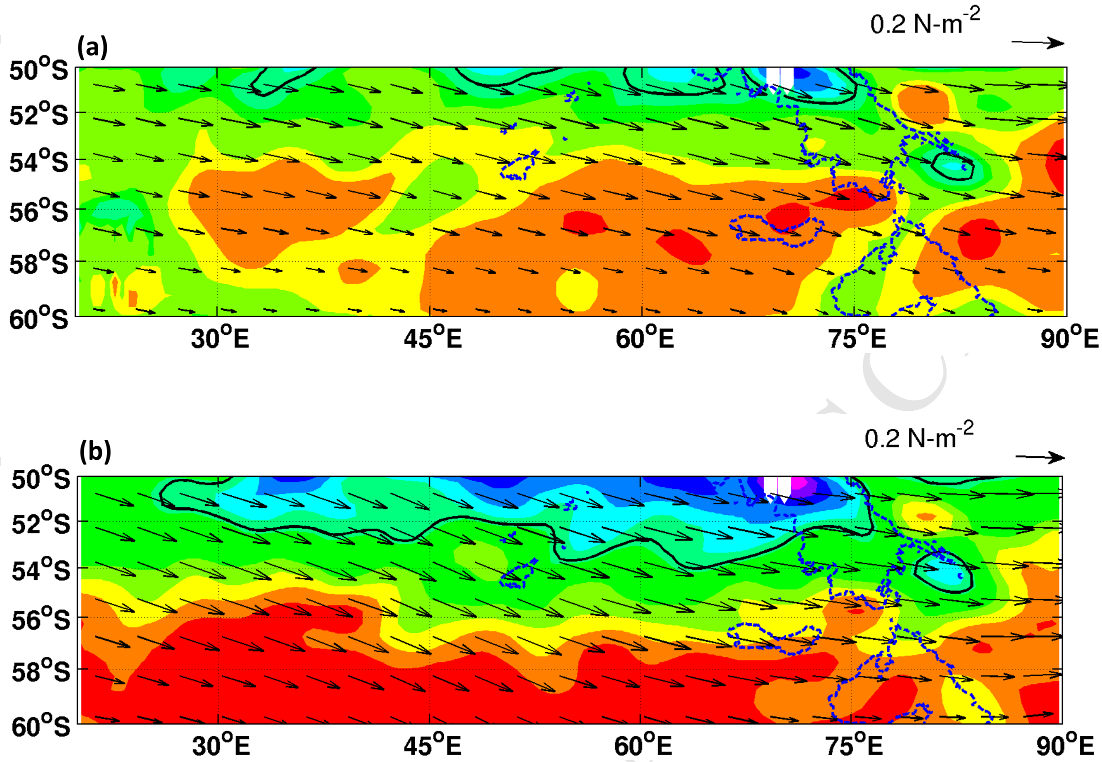

Fig. 6. Horizontal distribution of average wind stress curl (shaded, in Nm^{-3}) with wind stress vectors (vectors, in Nm^{-2}) overlaid on it, for (a) summer (December-January) and (b) autumn (February-March) over the study area.

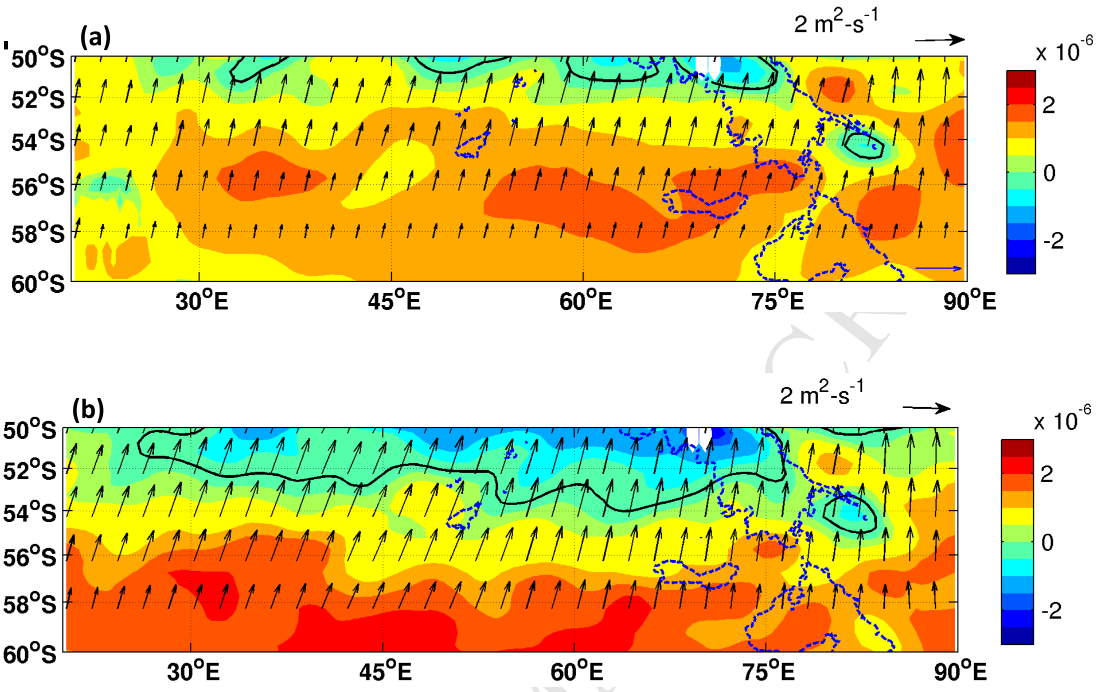

Fig. 7. Horizontal distribution of average Ekman pumping (shaded, in ms^{-1}) with Ekman transport (vectors, in m^2s^{-1}) overlaid on it, for (a) summer (December-January) and (b) autumn (February-March) over the study area.

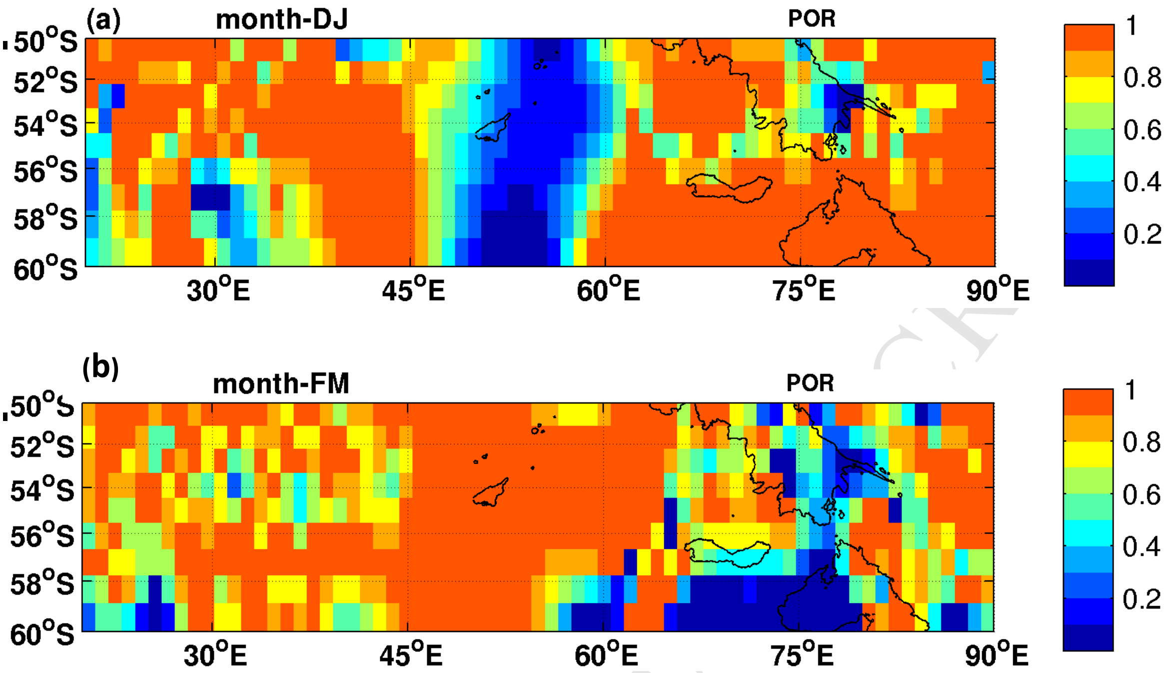

Fig. 8. Horizontal distribution of average barrier layer porosity (dimensionless) for (a) December-January months and (b) February-March months over the study area.

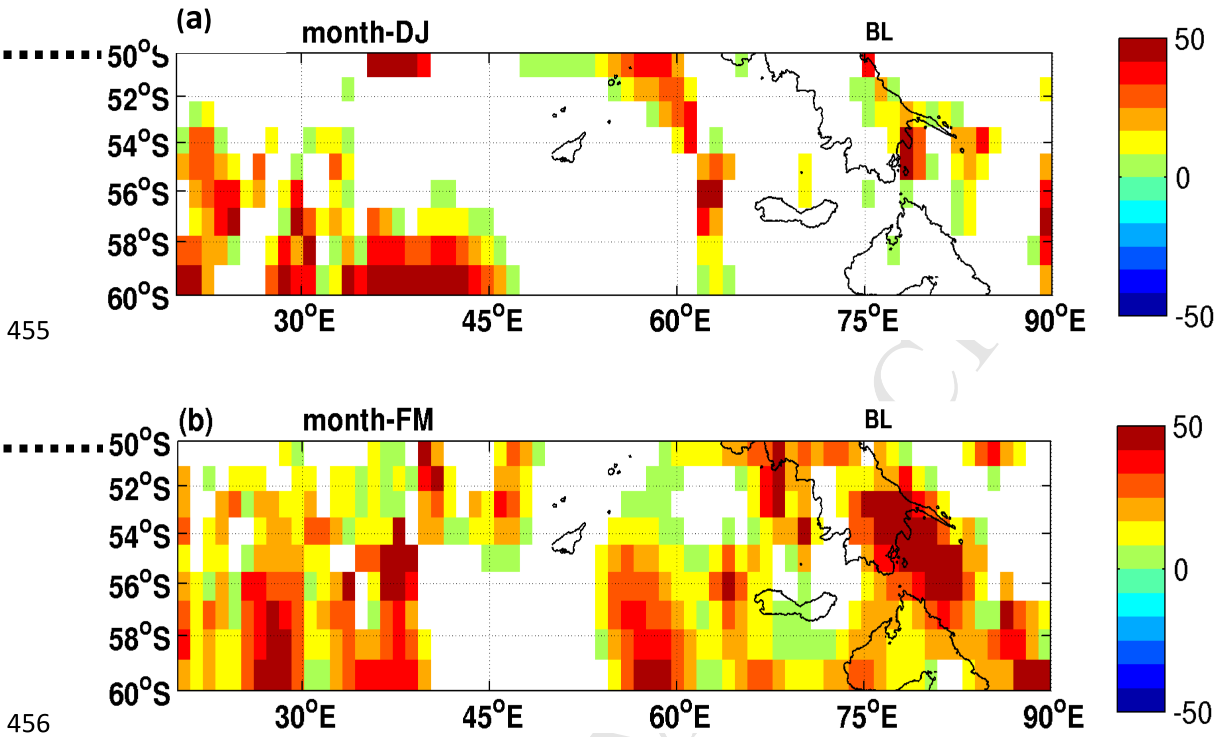

Fig. 9. Horizontal distribution of average barrier layer depth (in m) for (a) December-January months and (b) February-March months over the study area.

Figure Captions:

Fig. 1: Inter-annual variation of profile numbers with monthly distribution; blue part of the bar shows number of profiles in December, sky-blue part shows the same in January, yellow part shows the number of profiles in February while the red part represents the number of profiles in March for that particular year.

Fig. 2: The inner figure shows the study area is shown with a thick solid rectangular box. The colour bar represents the bathymetry of the region. The dashed box shows the Indian Ocean sector of the Southern Ocean Parkinson and Cavalieri (2012). The outer figure shows the schematic diagram of the circulation over the Fawn trough (FT) region (following van Wijk et al., 2010); red arrows show the Antarctic Circumpolar Current (ACC), green arrows show the Northern Polar Front (NPF) and blue arrows show the Southern polar Front (SPF).

Fig. 3: Typical temperature (left) and salinity (right) profile over (a) the Enderby Basin and (b) over the Australian-Antarctic Basin for regions to the south of Polar front. Upper (lower) panel represent the EB (AAB).

Fig. 4: Horizontal distribution of average isothermal layer depth (ILD, in m) calculated from in-situ observations between 1975 and 2012 for (a) summer (December-January) and (b) autumn (February-March) seasons over the study area.

Fig. 5: Horizontal distribution of average density mixed layer depth (MLD, in m) calculated from in-situ observations between 1975 and 2012 for (a) summer (December-January) and (b) autumn (February-March) over the study area.

Fig. 6: Horizontal distribution of average wind stress curl (shaded, in Nm-3) with wind stress vectors (vectors, in Nm-2) overlaid on it, for (a) summer (December-January) and (b) autumn (February-March) over the study area.

Fig. 7: Horizontal distribution of average Ekman pumping (shaded, in ms-1) with Ekman transport (vectors, in m2s-1) overlaid on it, for (a) summer (December-January) and (b) autumn (February-March) over the study area.

Fig. 8: horizontal distribution of average barrier layer porosity (dimensionless) for (a) December-January months and (b) February-March months over the study area.

Fig. 9: horizontal distribution of average barrier layer depth (in m) for (a) December-January months and (b) February-March months over the study area.